ELSEVIER

Journal of Nuclear Materials 288 (2001) 20–28

journal of nuclear materials

www.elsevier.nl/locate/jnucmat

Rim structure formation of isothermally irradiated UO_2 fuel discs

K. Une [a,*], K. Nogita [a,1], T. Shiratori [b], K. Hayashi [c]

[a] *Nippon Nuclear Fuel Development Co. Ltd., 2163 Narita-cho, Oarai-machi, Higashi Ibaraki-gun, Ibaraki-ken 311-1313, Japan*
[b] *Japan Atomic Energy Research Institute, Shirane 2-4, Shirakata, Tokai-mura, Naka-gun, Ibaraki-ken 319-1195, Japan*
[c] *Japan Atomic Energy Research Institute, 3607 Narita-cho, Oarai-machi, Higashi Ibaraki-gun, Ibaraki-ken 311-1394, Japan*

Received 18 June 2000; accepted 2 November 2000

Abstract

UO_2 fuel discs, which had been irradiated at an isothermal condition of 550–630°C to 51, 86 and 90 GWd/t without any restraint pressure, have been subjected to detailed microstructure observations, elemental analyses and density measurements. Their data were compared with previously reported results of high-burnup Zircaloy-clad type fuel pellets, so as to clarify the effect of pellet–cladding interaction (PCI) restraint on the rim structure formation. The porous rim structure, accompanying huge bubbles and high porosity, was recognized for the high-burnup discs of 86 and 90 GWd/t, but not for the 51 GWd/t disc. From the good coincidence between porosity increase and density decrease for the high-burnup discs, it was concluded that the precipitation and growth of coarsened rim bubbles substantially caused fuel swelling. The wide variety of rim bubble sizes and porosities at a given local burnup, which was recognized in the present PCI-free discs and Zircaloy-clad type pellets reported in other literature, possibly resulted from the external PCI restraint effect. The pressure difference between bubble internal and external pressures, and vacancy diffusivity would rate-control the growth of rim bubbles. © 2001 Elsevier Science B.V. All rights reserved.

PACS: 28.41.B; 61.80

1. Introduction

The rim structure region in high-burnup UO_2 fuels, which is characterized by increased porosity due to newly formed coarsened bubbles, Xe concentration depression from the matrix and grain subdivision of recrystallized grains with high-angle boundaries, tends to develop into the pellet inside region on increasing burnup. This microstructure change must influence integrated fuel performance at high burnups through the increases of fission gas release, fuel swelling and fuel temperature [1].

According to our proposed formation mechanism of the rim structure [1–3], extremely tangled dislocation networks are organized into the nuclei for recrystallized or sub-divided grains. Then, the coarsened rim bubbles are formed by sweeping out of fission gas atoms and small intragranular bubbles during grain growth on recrystallization and by short-range fission gas diffusion along recrystallized grain boundaries. Therefore, the rim bubbles are expected to contain fission gases at high pressures, exceeding the equilibrium values, due to the surface tension forces implied by dislocation punching [1,4]. A depression in Xe concentrations measured by electron probe microanalysis (EPMA) in the rim structure region results from the lowering of EPMA sensitivity for Xe enclosed in larger bubbles [5].

* Corresponding author. Present address: Japan Nuclear Fuel Co. Ltd., 2163 Narita-cho, Oarai-machi, Higashi Ibaraki-gun, Ibaraki-ken 311-1313, Japan. Tel.: +81-29 267 9012; fax: +81-29 266 2589.

E-mail address: une@nfd.co.jp (K. Une).

[1] Present address: Department of Mining, Minerals and Materials Engineering, The University of Queensland, Brisbane, QLD 4072, Australia.

0022-3115/01/$ - see front matter © 2001 Elsevier Science B.V. All rights reserved.
PII: S0022-3115(00)00712-1

Moreover, when increasing burnup, the pellet–cladding gap tends to close due to fuel swelling and cladding creep down, and it eventually forms a bonding layer [1]. Then any dimensional changes of the pellet (thermal expansion and swelling) are transmitted directly to the cladding tube, namely severe pellet–cladding interaction (PCI) arises. Under these conditions, the growth of the rim bubbles in the pellet outside region may be suppressed by strong PCI restraints, as in the case of fission gas bubbles in the pellet central region at high temperature. If this is the case, the gas pressure in the rim bubble and irradiation-induced diffusivity of vacancies might control its growth rate.

In recent years, many data regarding the development of rim structure, e.g., porosity, rim width and swelling, have been obtained for Zircaloy-clad type UO_2 fuel pellets which were irradiated in LWRs or test reactors with LWR conditions [1–4,6–21]. In these irradiation tests, PCI restraint forces are more or less imparted to the pellets during irradiation, depending on fuel rod design and burnup. In general, the higher the burnups are, the higher the restraint forces. In order to elucidate the effect of PCI restraint on the rim structure formation, the data of PCI-free fuels are desirable. However, quantitative information has been very limited so far. In the present study, PCI-free disc type UO_2 fuels were isothermally irradiated at about 550–630°C to a burnup range of 51–90 GWd/t, and they were subjected to detailed post-irradiation examinations (PIEs). The effect of PCI restraint was discussed by comparing the development of rim structure formation in the present disc specimens and in LWR and test reactor-irradiated fuel pellets.

2. Experimental

2.1. Specimens

In order to obtain UO_2 fuel specimens irradiated at an isothermal condition with almost no restraint pressure, fuel discs of 2.6-mm diameter and 1-mm thickness, which were sandwiched with Mo discs of 1.5-mm thickness, were irradiated in the JRR-3 test reactor of Japan Atomic Energy Institute (JAERI). The ^{235}U enrichments of the UO_2 powder used were 10.0 and 19.8 wt% to attain high burnup during a short period. The grain size and sintered density were 29 μm and 95.9% TD for the 10% enrichment discs, and 19 μm and 94.2% TD for the 19.8% enrichment discs.

A fuel stack consisting of 17 fuel discs was inserted into a Nb–1% Zr alloy cladding tube of 8-mm outside diameter and 109-mm length, in which He–5% Ar of 0.1 MPa was filled. This type of short pin was loaded into the irradiation capsule of the BRF-13H. The irradiation temperature was controlled by changing gas composition of a He and N_2 mixture between the inner and outer stainless-steel shell tubes, and continuously monitored by thermocouples attached on the cladding tube. The temperature difference between the cladding tube and fuel discs was estimated to be about 100°C by a one-dimensional temperature calculation code. The fuel disc temperature was kept nearly constant during the whole irradiation period; it was 550–630°C, except for 650–680°C at the beginning of irradiation. The duration of the irradiation was 257 effective full power days. The achieved fuel burnups were 51 GWd/t for the 10% enrichment discs, and 86 and 90 GWd/t for the 19.8% enrichment discs. Burnup measurements were carried out by both chemical analysis and gamma-ray spectroscopy. The average fission rates estimated from the irradiation duration and burnups are about 5.8×10^{13} for the 51 GWd/t discs and 1.0×10^{14} fissions/cm^3/s for the 86–90 GWd/t discs.

2.2. PIEs

The fuel microstructures were examined by optical microscopy (OM) and scanning electron microscopy (SEM) on a polished surface, by SEM on a fractured surface prepared by a diamond scratch method, and by transmission electron microscopy (TEM) on an argon ion-thinned specimen. Details of the specimen preparation for TEM have been described in [3]. In addition to the microstructural observation, crystallographic relations of rim structure region for higher-burnup specimens were investigated by using the selected area diffraction method of TEM. Fission products (FPs) of Xe, Cs and Ce retained in the fuel were analyzed by electron probe microanalysis (EPMA) with an electron beam diameter of 30 μm. Relative FP concentrations were obtained by dividing each characteristic X-ray intensity by that of uranium at the same location, so as to eliminate any effect from irregularity of the specimen surface. Fuel swelling of the disc specimens was examined by immersion density measurement using tetrabromo-ethylene (density: 2.965 g/cm^3 at 20°C).

The extent of rim structure formation was evaluated in terms of the increase in porosity obtained by OM and SEM, the swelling by density measurements, the subdivided grain structure obtained by SEM fractography, the fractional recrystallization area obtained by TEM, and the Xe concentration depression obtained by EPMA. The last technique originates from the significant lowering of EPMA sensitivity for Xe enclosed in the rim bubbles [5]. Among the above techniques, the three indexes of porosity, swelling and Xe depression are suitable for the quantitative evaluation of rim structure formation in the fuel specimens, since the three phenomena are directly related to the formation of coarsened rim bubbles [1,19,20].

3. Results

3.1. Ceramography and SEM

Figs. 1(a) and (b) show the ceramograph and SEM of an as-polished surface in the outermost region ($r/r_o = 0.95$–1.0) for the unirradiated disc which was prepared with 19.8% enriched uranium, and Figs. 1(c) and (d) are the corresponding photos for the 90 GWd/t disc. In the unirradiated disc, as-fabricated pores with round and smooth surface are observed, and the maximum pore size appears to be about 2–3 μm. By contrast, in the 90 GWd/t disc, there are many bubbles from sub-micron size to a maximum 5–6 μm with irregular surface, which is a characteristic feature of the rim structure. It is of particular interest that the bubble inner surface is irregular even for the sub-micron size bubbles. Some bubbles grow enormously and coalesce with each other, forming peanut-shaped bubbles. The maximum bubble size of 5–6 μm for the high-burnup disc specimen is about 2–3 times larger than the size reported in usual fuel pellets with almost the same burnup of 90 GWd/t [14,15,20].

Fig. 2 compares the pore or bubble size distributions per diameter class obtained from the ceramographs of the unirradiated and 90 GWd/t discs. The feature resolution limit by image analysis was about 0.6 μm. For the 90 GWd/t fuel, the bubble number density considerably increases and the size distribution shifts to a larger side, due to the nucleation and growth of rim bubbles. Resultant porosities based on the ceramographs are 5.2% and 17.5% for the unirradiated and 90 GWd/t fuels, respectively. The porosity is considerably increased by the precipitation and coarsening of rim bubbles. The porosity and bubble size distribution for the 90 GWd/t disc are nearly equivalent along the disc radial direction, indicating that the restructuring occurs almost uniformly throughout the disc. In another high-burnup disc of 86 GWd/t, almost the same microstructure change occurs: the porosity in this disc outside region is 15.2%.

SEMs of scratched surfaces in the outermost region of the 51 and 90 GWd/t discs are shown in Figs. 3(a) and

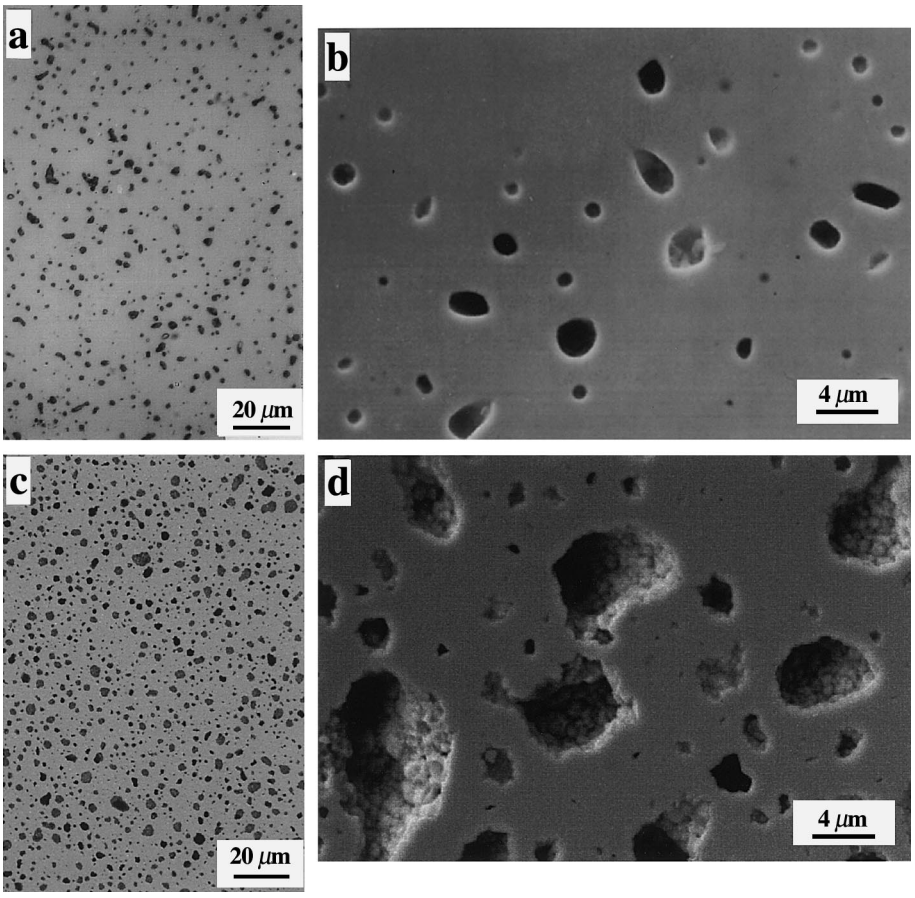

Fig. 1. Ceramographs and SEMs of as-polished surface at the outermost region of the unirradiated ((a) and (b)) and 90 GWd/t fuel discs ((c) and (d)).

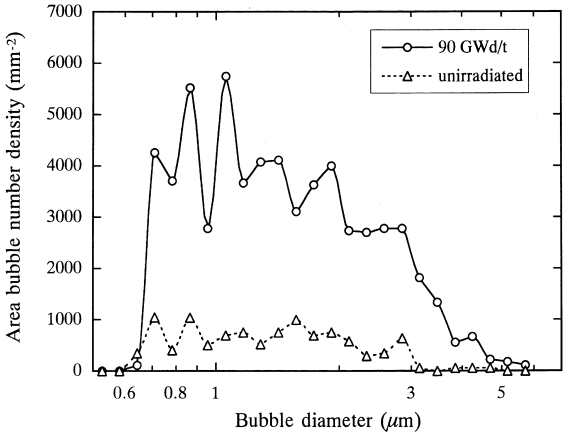

Fig. 2. Bubble size distributions of the unirradiated and 90 GWd/t fuel discs.

(b), respectively. In the 51 GWd/t disc, as-fabricated grain structure still remains, and no large grain boundary bubbles are observed, because of the low irradiation temperature of 550–630°C. The present result is compatible with the previously reported threshold burnup of about 70 GWd/t for the rim structure formation accompanying coarsened rim bubbles and developed sub-divided grains [10]. However, careful observation of Fig. 3(a) shows that sub-divided grains of about 0.3–0.4 μm size are concentrated on the inner surface of large as-fabricated pores and near the grain boundaries. This characteristic feature is not only seen in the isothermally irradiated fuel disc, but also in ordinary fuel pellets irradiated in LWRs or test reactors [8,14,15,17,19–21]. In the 90 GWd/t disc of Fig. 3(b), a highly developed sub-divided grain structure of about a half micron is clearly seen. On the inner surface of the coarsened rim bubbles of several microns size, the so-called cauliflower structure is clearly observed. These characteristic features also closely parallel the rim structure observed in the usual fuel pellets with high burnups, except for the huge sizes of the rim bubbles in the present fuel disc.

3.2. TEM

Fig. 4 shows a bright-field TEM image and a selected area electron diffraction (SAD) pattern with an area diameter of 600 nm. The TEM specimen was taken from the outside region of the 90 GWd/t disc. The SAD pattern does not show the main spots from the UO_2 single crystal, but rather indicates the presence of many recrystallized grains of 100–400 nm size with high-angle boundaries. These recrystallized grain sizes are in agreement with the results obtained in the rim region of BWR (average burnup: 49 GWd/t) [3], PWR (48 GWd/t) [12], PWR-type (83 GWd/t) [1,11] and the Halden boiling water reactor (HBWR) (60 GWd/t) pellets [16]. In the matrix of the recrystallized grains, a high density of small bubbles with about 2-nm size forms though almost no dislocations are present. On the grain boundaries of some new grains, small intergranular bubbles of several nanometers precipitate, and some of them are interconnected. These findings are also in accordance with the previous TEM examinations on LWR pellets [3,12]. TEM observation results show that the recrystallization process for the disc specimens is basically similar to that of the above high-burnup pellets, though the morphology and size of coarsened rim bubbles differ considerably.

Fig. 5 shows a bright-field TEM image in the region neighboring a rim bubble. On the inner surface of the bubble, the round-shaped cauliflower structure, which is observed in the SEM fractograph of Fig. 3(b), appears distinctly. Each grain of several hundred nanometers seems to be composed of many finer sub-grains of about 10 nm. These fine grains may correspond to the nuclei for new recrystallized grains.

3.3. Swelling

The densities measured by the Archimedes method for the present fuel discs are summarized in Table 1, together with porosity data measured by image analysis on the ceramographs. Swellings evaluated by both

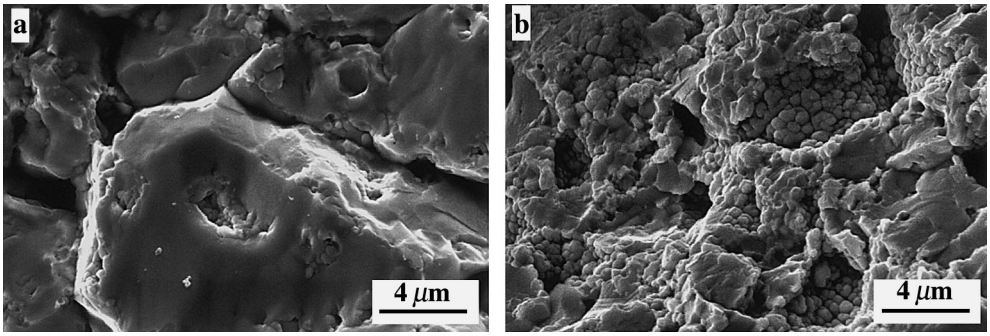

Fig. 3. SEM fractographs at the outermost region of the 51 GWd/t (a) and 90 GWd/t fuel discs (b).

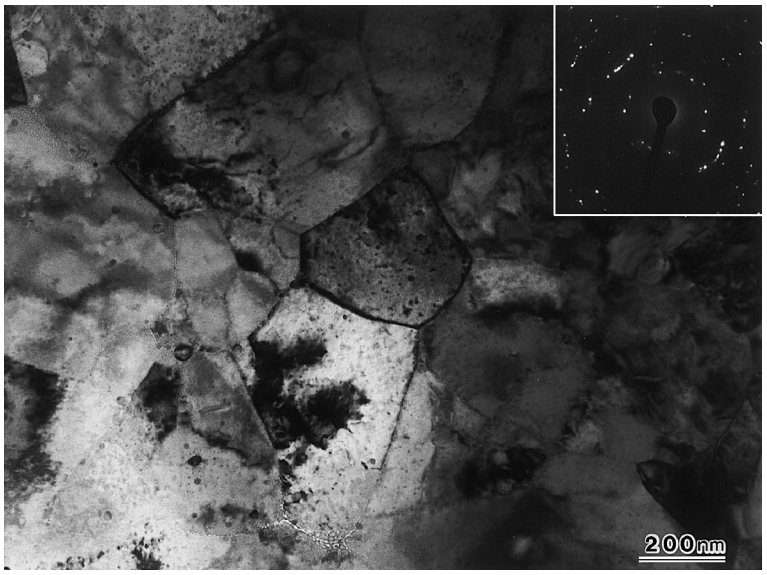

Fig. 4. Bright-field TEM image at the outermost region of the 90 GWd/t fuel disc. Insert: SAD pattern.

density and porosity changes between unirradiated and irradiated states are also listed.

A significant decrease of density or very large swelling of 19.3% for the 90 GWd/t disc is mostly attributed to precipitation of the huge rim bubbles. From Table 1, the values of the density swelling are generally larger than those of the porosity swelling. This is because the density swelling contains the contribution from matrix or solid fission product swelling, in addition to bubble swelling. Assuming the matrix swelling rate of 0.5–0.7% per 10 GWd/t, which has been sometimes applied to commercial LWR fuels irradiated up to 40–50 GWd/t [22,23], the swelling mainly caused by the rim bubbles (rim bubble swelling) becomes 13.0–14.8% for the 90 GWd/t disc. These values are close to the porosity increase of 12.3% from the unirradiated state. This demonstrates that the precipitation of coarsened rim bubbles substantially causes fuel swelling. In other words, a sufficient flow of vacancies is certainly accompanied by the growth of rim bubbles, as in the case of the growth

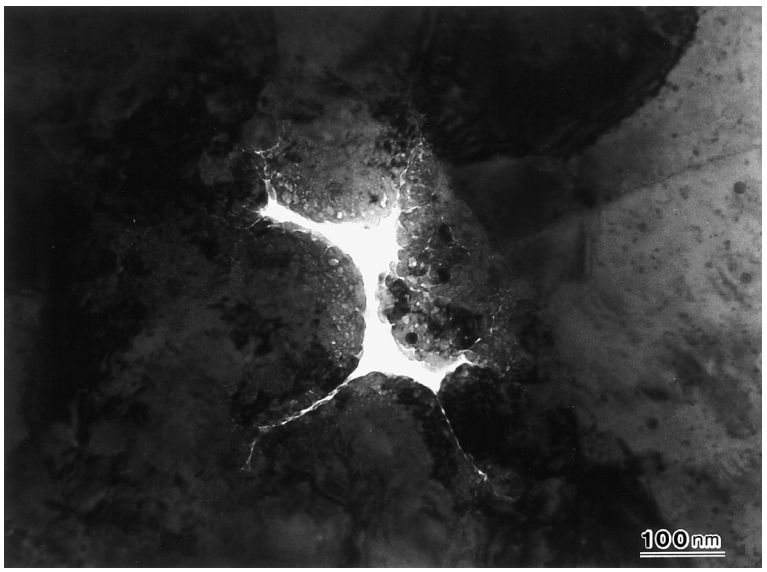

Fig. 5. Bright-field TEM image around a coarsened rim bubble in the 90 GWd/t fuel disc.

Table 1
PIE results of fuel discs[a]

Fuel disc	Burnup (GWd/t)	Density (g/cm^3)	Theoretical density (% TD)	Porosity (%)	Density swelling (%)	Porosity swelling (%)	Xe depression[b] (%)
Unirradiated[c]	0	10.51	95.9	3.9	–	–	–
Unirradiated[d]	0	10.32	94.2	5.2	–	–	–
Irradiated (D5)[c]	51	10.13	92.4	3.2	3.8	−0.7	1.9
Irradiated (B9)[d]	86	nm	nm	15.2	nm	10.0	70.0
Irradiated (F10)[d]	90	8.65	78.9	17.5	19.3	12.3	67.0

[a] nm: Not measured.
[b] Evaluated from Xe profiles by EPMA.
[c] Prepared with 10.0% enriched uranium.
[d] Prepared with 19.8% enriched uranium.

of fission gas bubbles observed in the high-temperature pellet central region.

For the case of the 51 GWd/t disc, the matrix swelling would be around 2.6–3.6%, which is close to the density swelling of 3.8%. This indicates that the rim bubble swelling was nearly zero. Actually, no typical rim bubble formation was observed in the disc, as shown in the fractograph of Fig. 3(a).

3.4. Xe depression

The radial distributions of Xe, Cs and Ce measured by EPMA for the 51 and 90 GWd/t discs are shown in Figs. 6(a) and (b), respectively. The Ce profile of rare earth element represents radial burnup profiles in the discs. From the measured Ce profiles, burnup in the discs is confirmed to be fairly flat, because highly enriched UO_2 of 10.0 or 19.8 wt% was used. In the figures, the generated Xe profiles are also given, which were estimated by the previously obtained relationship between characteristic X-ray intensity of Xe measured in the pellet outside region and burnup for various LWR and test reactor-irradiated pellets.

In the 51 GWd/t disc, fairly flat profiles of Xe and Cs are detected in the whole radial region of the disc. This indicates almost no release for gaseous and volatile fission products. Indeed, the Xe depression, which is defined as the fraction of depressed Xe concentration from the generated Xe concentration, is nearly zero.

In the 90 GWd/t disc, the Xe concentrations in the outermost region of about 200 μm near the disc surface are somewhat lower than in the inside region. By contrast, this kind of lowering in the Cs profile is not detected. This indicates that the Xe lowering in the outermost region results from a little more developed rim structure formation, not by Xe release from the disc. The average Xe depressions in the whole radial region of the disc are 67% for the 90 GWd/t specimen and 70% for the 86 GWd/t specimen. These values are close to the

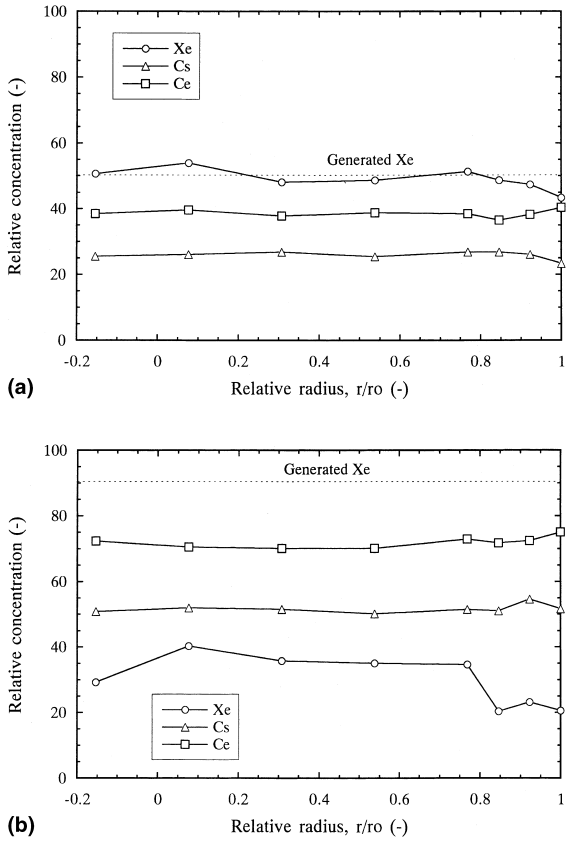

Fig. 6. (a) Radial distributions of relative FP concentration for the 51 GWd/t fuel disc.(b) Radial distributions of relative FP concentration for the 90 GWd/t fuel disc.

average depressions in the outside region ($r/r_o = 1.0$–0.8) previously measured for PWR-type (83 GWd/t) [1,11] and HBWR (86 GWd/t) pellets [19,20], which were 55% and 62%, respectively. This coincidence probably implies that almost the same extent of recrystallization occurs in both the present fuel disc and the fuel pellets with burnups of around 83–90 GWd/t.

4. Discussion

Fig. 7 shows the relationship between porosity and Xe depression in the rim structure region of the present fuel disc and the Zircaloy-clad type fuel pellets reported in the literature [9,11,17,20]. Indeed, comparing the micrographs and bubble size distributions for the present disc of 90 GWd/t without any restraint pressure and the HBWR pellet of 86 GWd/t with a severe PCI restraint [20, Figs. 1 and 3], significant differences in porosity and rim bubble size are observed, in spite of almost the same Xe depressions or rim structure formation for both specimens. For example, the Xe depressions for the present discs and the HBWR pellets are similar and around 62–70%, while the porosities are 15–18% for the disc and 6–8% for the pellet specimens. Moreover, the maximum bubble sizes are about 5–6 μm for the former and 2–3 μm for the latter specimens.

This difference is probably due to the effect of restraint pressure during irradiation, not to the differences in fuel fabrication history and other irradiation conditions (temperature, fission rate, etc.). Actually, the HBWR fuel rods above 60 GWd/t showed large cladding residual strains of 1.2–1.4%, and the bonding layer between pellet and cladding was almost fully formed [24]. These indications evince that a severe PCI occurred during the irradiation. On the other hand, in the case of the JRR-3 fuel discs, stack weight was only loaded to the discs.

The correlation between local burnup and porosity for the present discs is plotted in Fig. 8, together with other literature data [9,11,14,15,17,20]. Of course, careful attention is required in comparing various porosity data obtained from different methods for quantitative image analysis and different pellet initial porosities. For example, the initial porosities are 5.2% for the present disc and 2.3% for the HBWR pellets [20]. In Fig. 8, the

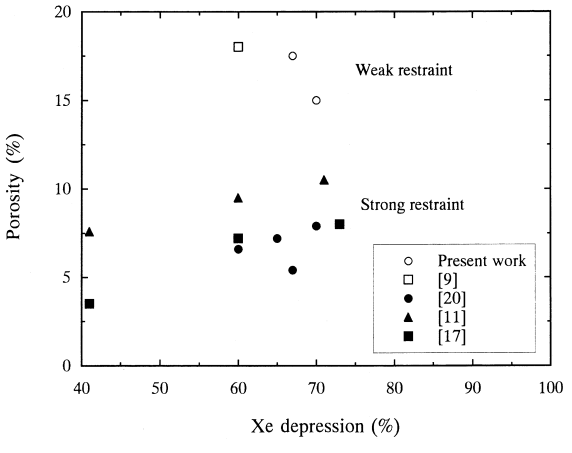

Fig. 7. Relationship between Xe depression and porosity.

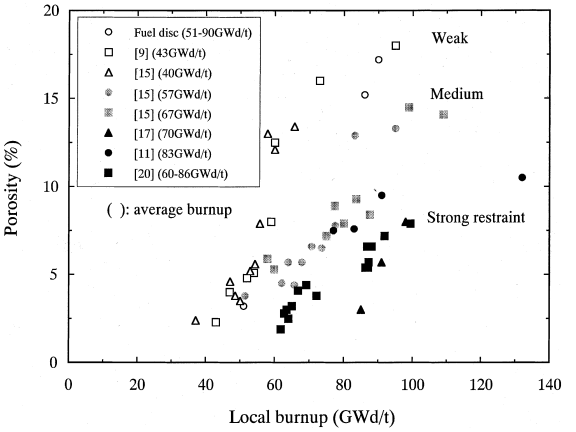

Fig. 8. Relationship between local burnup and porosity.

porosities appear to increase with higher burnups, roughly following three different curves, and to saturate at the values of 8–18% around 100 GWd/t. In fact, a clear saturation effect has been noticed for PWR fuel pellets, in which the porosity at the pellet edge was saturated at a level of 13–14% though the pellet average burnup increased from 40 to 67 GWd/t [14,15]. Obviously, the present disc data belong to the highest porosity curve and the previous HBWR pellet data to the lowest curve. There are differences of two or three factors for porosity at 100 GWd/t between the highest (weak restraint) and the lowest (strong restraint) curves. For the fuel pellets that are categorized as the weak restraint condition, no bonding layer formation has been confirmed. By contrast, for the pellets that fall under the medium and strong restraint conditions, its formation was reported.

The above restraint effect on the rim porosity or rim bubble growth may be explained by the Hull and Rimmer model [25], which has been frequently applied to the growth kinetics of fission gas bubbles observed in the high-temperature pellet central region. Their growth rate is proportional to vacancy diffusivity along a grain boundary and the pressure difference between the bubble internal and external pressures, i.e. $dr/dt \propto D_v \Delta p$. A sufficient flow of vacancies along vacancy potential would be supplied by fission cascade process, besides thermal process. The pressures in the rim bubbles of several hundred nanometers to micron sizes have been estimated to be about 100–150 MPa [1,4] to several ten MPa [14]. These values certainly exceed their thermodynamic equilibrium pressures of several MPa. On the other hand, the magnitude of the PCI restraint pressure in the pellet during power transient condition has been calculated to be more or less 90 MPa [26]. Therefore, when external or PCI restraint pressure is weak, strong excess pressure can lead to the growth of rim bubbles

even at lower temperatures below 1000°C. By contrast, when strong PCI restraint is imparted to the pellet outside region at high burnups, the bubble growth may be suppressed or the bubbles may shrink. Consequently, the rim bubble porosity and bubble size do not monotonously increase with increasing burnup. Rather, they are suppressed or reduced at higher burnups, though the porous rim structure region develops towards the pellet inside region.

5. Conclusions

The UO_2 fuel discs, which had been irradiated at an isothermal condition of 550–630°C to 51–90 GWd/t without any restraint pressure, were subjected to detailed microstructure observations, elemental analyses and density measurements. Their data were compared with the previously reported data of high-burnup fuel pellets irradiated in LWRs or test reactors.

The formation of highly developed porous rim structure was recognized for the high-burnup discs of 86–90 GWd/t, while almost no microstructural change was observed for the 51 GWd/t disc. The present results were compatible with the reported threshold burnup of about 70 GWd/t for the rim structure formation. The porosities of the high-burnup discs were very high at a level of 15–18% in almost the entire region of the discs. The rim bubbles grew enormously to a maximum size of 5–6 μm. Despite the unusual growth of rim bubbles, their recrystallized grain size of 100–400 nm was equivalent to that of Zircaloy-clad type fuel pellets. The porosity increase from the as-fabricated state was in good accordance with fuel swelling after subtracting the contribution of matrix swelling (0.5–0.7% per 10 GWd/t). This demonstrated that the precipitation of coarsened rim bubbles substantially contributed to fuel swelling. In other words, a sufficient flow of vacancies was certainly accompanied by the growth of rim bubbles.

The morphology of rim bubbles for the disc specimens was very different from that for the previously obtained high-burnup pellets with severe PCI restraint, which had been irradiated to 86 GWd/t in the Halden reactor, although the extent of rim structure formation (or Xe depression) was almost the same for both types of fuels. In the fuel pellets, maximum bubble size and porosity in the pellet outside region were suppressed to about 2–3 μm and 7–8%, respectively. The wide variety of rim bubble sizes and porosities, which was recognized in the above two types of fuel specimens and LWR fuel pellets in other literature, possibly resulted from the external restraint effect. The pressure difference between bubble internal and external PCI pressures and vacancy diffusivity would rate-control the growth of rim bubbles.

References

[1] K. Une, K. Nogita, S. Kashibe, T. Toyonaga, M. Amaya, in: Proceedings of the International Topical Meeting on LWR Fuel Performance, Portland, OR, 1997, p. 478.
[2] K. Nogita, K. Une, Nucl. Instrum. and Meth. B 91 (1994) 301.
[3] K. Nogita, K. Une, J. Nucl. Mater. 226 (1995) 302.
[4] K. Nogita, K. Une, Nucl. Instrum. and Meth. B 141 (1998) 481.
[5] C. Ronchi, C.T. Walker, J. Phys. D 13 (1980) 2175.
[6] M.E. Cunningham, M.D. Freshley, D.D. Lanning, J. Nucl. Mater. 188 (1992) 19.
[7] S.R. Pati, A.M. Garde, L.J. Klink, in: Proceedings of the ANS Topical Meeting on LWR Fuel Performance, Williamsburg, VI, 1988, p. 204.
[8] Hj. Matzke, H. Blank, M. Coquerelle, K. Lassmann, I.L.E. Ray, C. Ronchi, C.T. Walker, J. Nucl. Mater. 166 (1989) 165.
[9] S. Koizumi, H. Umehara, Y. Wakashima, in: Proceedings of the IAEA Technical Committee Meeting on Fuel Performance at High Burnup for Water Reactors, Nykoping, 1990, p. 102.
[10] C.T. Walker, T. Kameyama, S. Kitajima, M. Kinoshita, J. Nucl. Mater. 188 (1992) 93.
[11] K. Une, K. Nogita, S. Kashibe, M. Imamura, J. Nucl. Mater. 188 (1992) 65.
[12] L.E. Thomas, C.E. Beyer, L.A. Charlot, J. Nucl. Mater. 188 (1992) 80.
[13] R.P. Piron, B. Bordin, G. Geoffrey, C. Maunier, D. Baron, in: Proceedings of the International Topical Meeting on LWR Fuel Performance, West Palm Beach, FL, 1994, p. 321.
[14] J. Spino, K. Vennix, M. Coquerelle, J. Nucl. Mater. 231 (1996) 179.
[15] J. Spino, M. Coquerelle, D. Baron, in: IAEA Technical Committee Meeting on Advances in Pellet Technology for Improved Performance at High Burnup, Tokyo, October 1996.
[16] K. Nogita, K. Une, M. Hirai, K. Ito, K. Ito, Y. Shirai, J. Nucl. Mater. 248 (1997) 196.
[17] J. Spino, D. Baron, M. Coquerelle, A.D. Stalios, J. Nucl. Mater. 256 (1998) 189.
[18] M. Mogensen, J.H. Pearce, C.T. Walker, J. Nucl. Mater. 264 (1999) 99.
[19] K. Une, M. Hirai, K. Nogita, T. Hosokawa, Y. Suzawa, S. Shimizu, Y. Etoh, J. Nucl. Mater. 278 (2000) 54.
[20] K. Une, K. Nogita, Y. Suzawa, K. Hayashi, K. Itoh, Y. Etoh, in: Proceedings of the International Topical Meeting on LWR Fuel Performance, Park City, UT, 2000, p. 775.
[21] N. Lozano, L. Desgranges, D. Aymes, J.C. Niepce, J. Nucl. Mater. 257 (1998) 78.
[22] H. Ohara, T. Nomata, M. Irube, M. Futakuchi, S. Iwata, in: Proceedings of the International Topical Meeting on LWR Fuel Performance, West Palm Beach, FL, 1994, p. 674.
[23] T. Fujibayasi, S. Koizumi, K. Tsukui, T. Futami, T. Okubo, Y. Mishima, M. Oishi, T. Aoki, in: IAEA Specialists' Meeting on Postirradiation Examination and Experience, Tokyo, 1981.

[24] M. Hirai, T. Hosokawa, R. Yuda, K. Une, S. Kashibe, K. Nogita, Y. Shirai, H. Harada, T. Kogai, T. Kubo, J.H. Davies, in: Proceedings of the International Topical Meeting on LWR Fuel Performance, Portland, OR, 1997, p. 490.
[25] D. Hull, D.E. Rimmer, Philos. Mag. 4 (1959) 673.
[26] C.T. Walker, P. Knappik, M. Mogensen, J. Nucl. Mater. 160 (1988) 10.